



Power Electronic Systems
Laboratory

© 2012 IEEE

Proceedings of the 27th Applied Power Electronics Conference and Exposition (APEC 2012), Orlando Florida, USA,
February 5-9, 2012

Switching Control Strategy for Full ZVS Soft-Switching Operation of a Dual Active Bridge AC/DC Converter

J. Everts,
J. Van den Keybus,
F. Krismer,
J. Driesen,
J. W. Kolar

This material is published in order to provide access to research results of the Power Electronic Systems Laboratory / D-ITET / ETH Zurich. Internal or personal use of this material is permitted. However, permission to reprint/republish this material for advertising or promotional purposes or for creating new collective works for resale or redistribution must be obtained from the copyright holder. By choosing to view this document, you agree to all provisions of the copyright laws protecting it.



Eidgenössische Technische Hochschule Zürich
Swiss Federal Institute of Technology Zurich

Switching Control Strategy for Full ZVS Soft-Switching Operation of a Dual Active Bridge AC/DC Converter

Jordi Everts^{*‡}, Jeroen Van den Keybus[†], Florian Krismer[‡], Johan Driesen^{*}, and Johann W. Kolar[‡]

^{*}Dept. of Electrical Engineering ESAT-ELECTA
Katholieke Universiteit Leuven, Belgium
Email: jordi.everts@esat.kuleuven.be

[‡]Power Electronic Systems (PES) Laboratory
ETH Zurich, Switzerland

[†]TRIPHASE
Leuven, Belgium

Abstract—A switching control strategy to enable Zero-Voltage-Switching (ZVS) over the entire input-voltage interval and the full power range of a single-stage Dual Active Bridge (DAB) AC/DC converter is proposed. The converter topology consists of a DAB DC/DC converter, receiving a rectified AC line voltage via a synchronous rectifier. The DAB comprises primary and secondary side full bridges, linked by a high-frequency isolation transformer and inductor. Using conventional control strategies, the soft-switching boundary conditions are exceeded at the higher voltage conversion ratios of the AC input interval. Recently we presented a novel pulse-width-modulation strategy to fully eliminate these boundaries, using a half bridge - full bridge DAB configuration. In this paper the analysis is extended towards a full bridge - full bridge DAB setup, providing more flexibility to minimize the component RMS currents and allowing increased performance (in terms of efficiency and volume). Experimental results are given to validate the theoretical analysis and practical feasibility of the proposed strategy.

Index Terms—AC/DC converter, bidirectional, Dual Active Bridge, DAB, isolated, soft-switching, switching control strategy, Zero Voltage Switching, ZVS

I. INTRODUCTION

Utility interfaced isolated AC/DC converters cover a wide range of applications such as power supplies in telecommunication and data centers [1]–[3], plug-in hybrid electrical vehicles (PHEVs) and battery electric vehicles (BEVs) [4], [5]. Bidirectional functionality is increasingly required since the traditional electricity grid is evolving from a rather passive to a smart interactive service network (customers/operators) where the traditional central control philosophy is shifting towards a more distributed control paradigm and where the energy systems play an active role in providing different types of support to the grid [5], [6]. In this area of grid-interfaced systems, Dual Active Bridge (DAB) converters seem to be a favorable choice for complying with future system requirements [7], [8]. The biggest advantage of the DAB topologies

is that the AC/DC energy conversions can take place in a single conversion stage, producing high quality waveforms and complying with future regulations on low and high frequency distortions of the mains AC power lines without the need for increasing the size and reactance value of the passive filter elements and for a separate front-end power factor correcting converter [7], [8]. Therefore a DAB DC/DC converter is used in combination with a synchronous rectifier, realizing a single-stage, bidirectional AC/DC power converter [8]. The soft-switching DAB consists of two full bridges, interfaced by a high-frequency (HF) transformer, and was originally introduced in [7] for realizing high-efficiency and high-power-density, isolated DC/DC conversions with the capability of buck-boost operation and bidirectional power flow. It was shown in [8] that single-stage, unity power factor AC/DC conversions are possible by combining the DAB DC/DC converter with a diode bridge rectifier or a more efficient synchronous rectifier (for bidirectional operation). When using conventional control strategies [7]–[10], the efficient soft-switching (ZVS) region of the DAB DC/DC converter is restricted by its voltage conversion ratio. Full-power-range soft-switching operation is only possible when this ratio is equal to one. However, when being used in an AC/DC setup, the input voltage of the DAB is a rectified sinewave, implying a variable voltage conversion ratio and restricted soft-switching operation. Recently we presented a pulse-width-modulation strategy to eliminate these boundaries, allowing soft-switching operation over the entire input sinewave interval and power range [11]. In [11] a half bridge - full bridge DAB configuration was used. In this paper the analysis is extended towards a full bridge - full bridge DAB implementation, providing more flexibility to minimize the component RMS currents and allowing increased performance (in terms of efficiency and power density).

The single stage Dual Active Bridge (DAB) AC/DC converter topology is explained in Section II. Section III contains a comprehensive analysis of the DAB switching modes, including the derivation of the mode equations and soft-switching boundary conditions. The final switching control strategy that

This research is partly funded by a Ph.D. grant of the Institute for the Promotion of Innovation through Science and Technology in Flanders (IWT-Vlaanderen). Jordi Everts is a doctoral research assistant of IWT-Vlaanderen. Jordi Everts is also a visiting doctoral researcher at the Power Electronic Systems Laboratory, ETH Zurich, Switzerland (scholarship of FWO-Vlaanderen).

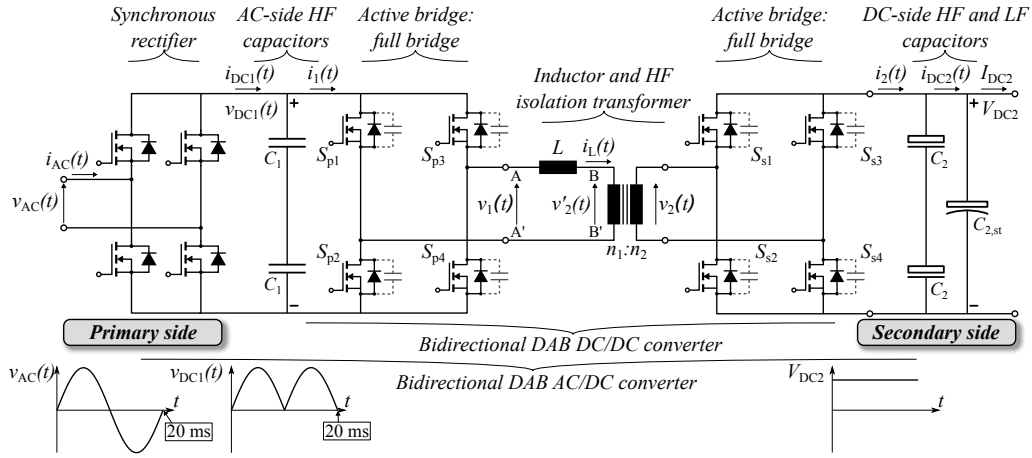


Fig. 1. Circuit schematic of the bidirectional, isolated DAB AC/DC converter topology.

allows to control the DAB AC/DC converter under full soft-switching is discussed in Section IV, followed by a topology evaluation in Section V. The analysis in this paper is based on the converter specifications provided in Table I.

TABLE I
CONVERTER SPECIFICATIONS

| Property | | Value |
|-----------|------------------|--|
| AC-side | $V_{AC,rms}$ | 230V (nominal) $207V \leq V_{AC,rms} \leq 253V$ |
| | $I_{AC,rms,nom}$ | 16A |
| DC-side | V_{DC2} | 400V (nominal) $360V \leq V_{DC2} \leq 440V$ |
| | f_s | 120kHz |
| n_1/n_2 | | 1 |
| L, L_M | | 11.2 μ H, 105.45 μ H |

II. DUAL ACTIVE BRIDGE AC/DC CONVERTER TOPOLOGY

Fig. 1 shows the schematic of the bidirectional, isolated DAB AC/DC converter topology. The rectified AC line voltage $v_{DC1}(t)$, coming from the synchronous rectifier, is directly fed to the DAB DC/DC converter, putting a small high-frequency (HF) filter capacitor C_1 in between. The DAB comprises HF transformer-coupled primary and secondary side full bridges, performing the DC output voltage (V_{DC2}) regulation while maintaining unity power factor at the AC side by actively wave-shaping the line current $i_{DC1}(t)$ [8]. Therefore they produce phase-shifted edge resonant square wave voltages $v_1(t)$ and $v_2(t)$ at the terminals of the HF AC-link (inductor L and HF transformer), resulting in an inductor current $i_L(t)$. Both active bridges act as AC/DC converters to their DC side, transforming the AC current $i_L(t)$ into net DC currents $i_1(t)$ and $i_2(t)$ on the primary respectively secondary side. After passing HF filter capacitors C_1 and C_2 , DC currents $i_{DC1}(t)$ and $i_{DC2}(t)$ are obtained. These two currents can be

phase aligned with $v_{DC1}(t)$ by proper control of the two active bridges, realizing the unity power factor:

$$i_{DC1}(t) = |I_{DC1} \sin(\omega_L t)| \quad (1)$$

$$v_{DC1}(t) = |V_{DC1} \sin(\omega_L t)| \quad (2)$$

with ω_L the 50Hz AC line frequency. The voltages $v_1(t)$ and $v_2(t)$ generated by the active bridges are square waves with a duty cycle of $\leq 50\%$.

As shown in Fig. 2 (right inset), each high-frequency switch S_{xx} is implemented by a power transistor T_{xx} , a diode D_{xx} , and a parasitic capacitor C_{xx} . Soft-switching operation occurs when a voltage transition is initiated by turn-off of the respective switch S_{xx} , commutating the current from the transistor T_{xx} to the opposite diode D_{xx} of the leg (e.g. commutation from T_{p1} to D_{p2}) [12], [13]. When this momentaneous resonant transition (quasi-resonant ZVS) completes, T_{p2} is turned on under ZVS (anti-parallel diode is conducting). It was shown in [12] that for high voltage MOSFETs a minimum turn-off commutation current of $I_{comm} \geq 2A$ is needed to recharge the parasitic drain to source capacitors within a 200ns dead-time interval, avoiding increased switching losses.

III. SWITCHING CONTROL ANALYSIS

The analysis of the switching sequences and control of the DAB AC/DC converter can in a first step be simplified by considering the magnetizing inductance L_M of the transformer to be much larger than the inductance L and by neglecting the

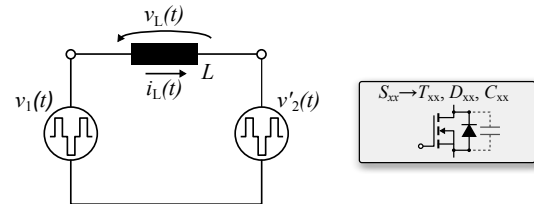


Fig. 2. Simplified model of the DAB (left inset), and representation of the high-frequency switches S_{xx} (right inset).

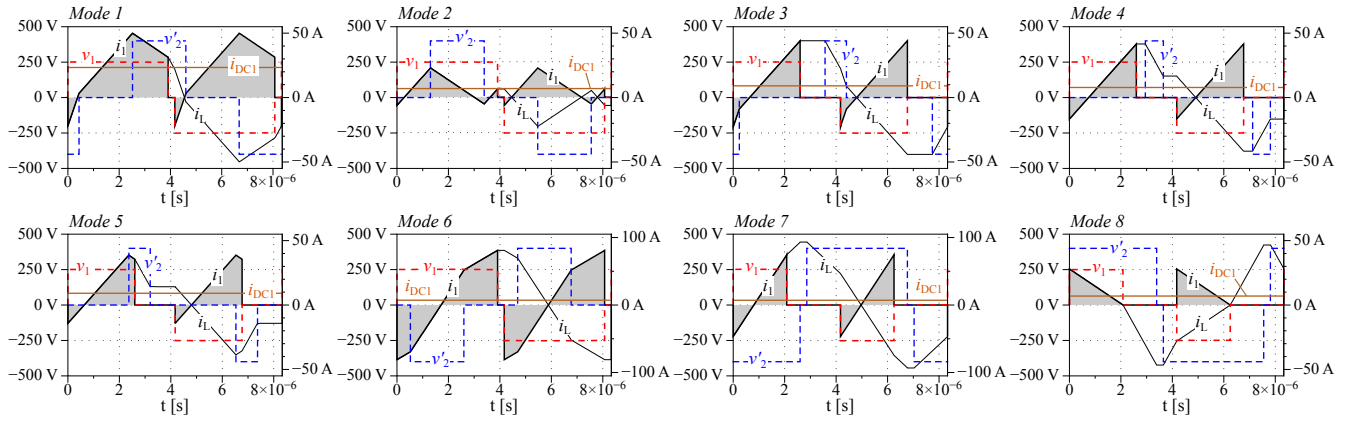


Fig. 3. Possible switching sequences and corresponding switching modes of the DAB topology for positive power flow ($i_{DC1} > 0$). The depicted waveforms are derived for: $f_s = 120\text{kHz}$, $v_{DC1} = 250\text{V}$, and $V_{DC2} = 400\text{V}$ (nominal DC output voltage).

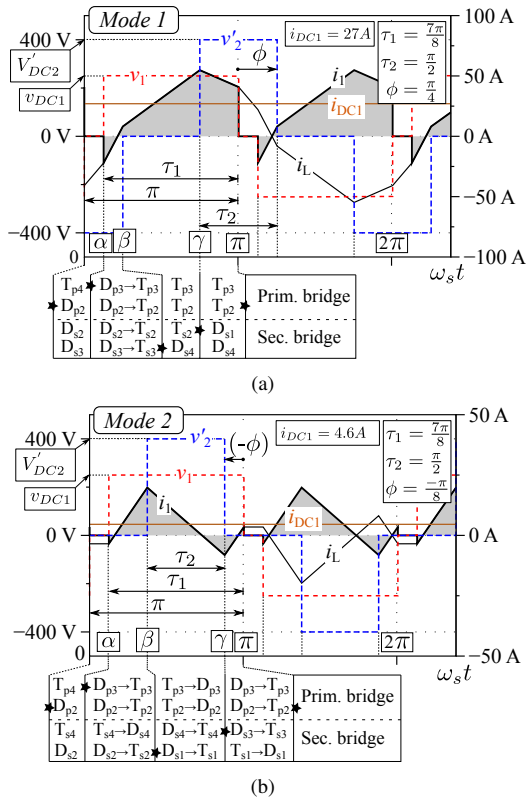


Fig. 4. Ideal voltages and current waveforms for mode 1 (Fig. 4(a)) and mode 2 (Fig. 4(b)) operation. The depicted waveforms are derived for: $v_{DC1} = 250\text{V}$, and $V_{DC2} = 400\text{V}$ (nominal DC output voltage).

transformer leakage inductances L_{lr1} and L_{lr2} . By referring the model to the primary side of the transformer, a simplified representation of the DAB is obtained (Fig. 2, left inset). The primary side referred voltage $v'_2(t)$ is given by:

$$v'_2(t) = v_2(t) \frac{n_1}{n_2} \quad (3)$$

For brevity, only power flow from the AC side (primary side) to the DC side (secondary side) is considered, denoted

as the positive power flow. The analysis for reverse power flow is similar. The power flow is controlled by applying an appropriate phase shift angle ϕ between the voltages $v_1(t)$ and $v'_2(t)$ and additionally controlling the pulse width modulation angles τ_1 and τ_2 of respectively $v_1(t)$ and $v'_2(t)$ (angles are defined in Figs. 4(a) and 4(b)).

A. Switching Modes

Depending on the sequence in time of the falling and rising edges of the voltages $v_1(t)$ and $v'_2(t)$, eight different switching modes can be distinguished for each power flow direction, as shown in Fig. 3 (positive power flow). The modes for negative power flow are similar. It can be observed from Fig. 3 that modes 2, 6, 7, and 8 also allow a negative power flow, resulting in a total of 12 possible switching modes for the DAB.

To determine the optimal control angles (ϕ , τ_1 , and τ_2) and the corresponding mode in every point of the 50Hz input sinewave, in a first step a selection/optimization algorithm was developed. The objective function (to be minimized) of this nonlinear, constrained optimization/selection problem is the equivalent RMS current $I_{S,eq,rms}$ in the high-frequency switches S_{xx} , defined as:

$$I_{S,eq,rms} = \sqrt{\frac{1}{\pi} \int_0^\pi (i_{S,rms}(\omega_L t))^2 d(\omega_L t)} \quad (4)$$

The choice of the objection function is justified as the switching losses for the soft-switching DAB are low, especially when assuring a minimum switch commutation current $I_{comm} \geq 2\text{A}$. The constraints of the algorithm are the current $i_{DC1}(t)$ (1), realizing the unity power factor, and the minimum commutation currents I_{comm} in the switches S_{xx} , guaranteeing soft-switching in every point of the 50Hz period. Moreover, the control angles ϕ , τ_1 , and τ_2 are constrained within their physical limits ($0 \leq \tau_1, \tau_2 \leq \pi$ and $-\pi \leq \phi \leq \pi$). By analyzing the outcome of the algorithm, it was seen that only two modes are preferably used in the sinewave interval (further referred to as mode 1 and mode 2, respectively depicted in Fig. 4(a) and Fig. 4(b))

and forming the basis of the strategy proposed in this paper. Intuitively this result could be expected as it can be seen from Fig. 3 that the remaining 6 options lead to an increased RMS value of the inductor current i_L and do not result in a higher DAB power level. Moreover, for modes 3, 4, 5, and 8 the soft-switching constraints are difficult, or sometimes even impossible to meet. Although the implementation of the optimization/selection algorithm required the equations (currents and soft-switching constraints) for all eight modes, for brevity only the derivation of the equations for the two most appropriate modes (mode 1 and mode 2) is given in the following. In addition to the determination of the optimal control angles ϕ , τ_1 , and τ_2 (inner loop), the design parameters L (inductance value) and n_1/n_2 (transformer ratio) are varied in an outer loop, resulting in the optimal $L = 11.2\mu\text{H}$ and $n_1/n_2 = 1$ shown in Table I.

When choosing ϕ as the angle between the first falling edge of $v_1(t)$ and the first falling edge of $v_2'(t)$, the transition between mode 1 and mode 2, occurs at $\phi = 0$. According to Figs. 2, 4(a), and 4(b), for each mode the dynamics of the inductor current $i_L(t)$ can be expressed as:

$$\frac{di_L(t)}{dt} = \frac{v_L(t)}{L} \quad (5)$$

with

$$v_L(t) = v_1(t) - v_2'(t) \quad (6)$$

Solving these equations for $i_L(t)$ in each interval defined in Figs. 4(a) and 4(b), and evaluating the resulting system of equations yields the expressions for i_L at the different switching instances $\theta = \{0, \alpha, \beta, \gamma, \text{ and } \pi\}$:

Mode 1

$$i_L(0) = \frac{-2\phi V'_{DC2} - \tau_1 v_{DC1} + \tau_2 V'_{DC2}}{2\omega_s L} = -i_L(\pi) \quad (7)$$

$$i_L(\alpha) = \frac{-2\phi V'_{DC2} - \tau_1(2V'_{DC2} + v_{DC1}) + \tau_2 V'_{DC2} + 2\pi V'_{DC2}}{2\omega_s L} \quad (8)$$

$$i_L(\beta) = \frac{2\phi v_{DC1} + \tau_1 v_{DC1} + \tau_2 V'_{DC2} + 2\pi v_{DC1}}{2\omega_s L} \quad (9)$$

$$i_L(\gamma) = \frac{2\phi v_{DC1} + \tau_1 v_{DC1} + \tau_2(V'_{DC2} - 2v_{DC1})}{2\omega_s L} \quad (10)$$

Mode 2

$$i_L(0) = \frac{-\tau_1 v_{DC1} + \tau_2 V'_{DC2}}{2\omega_s L} = -i_L(\pi) \quad (11)$$

$$i_L(\alpha) = \frac{-\tau_1 v_{DC1} + \tau_2 V'_{DC2}}{2\omega_s L} \quad (12)$$

$$i_L(\beta) = \frac{2\phi v_{DC1} + \tau_1 v_{DC1} + \tau_2(V'_{DC2} - 2v_{DC1})}{2\omega_s L} \quad (13)$$

$$i_L(\gamma) = \frac{2\phi v_{DC1} + \tau_1 v_{DC1} - \tau_2 V'_{DC2}}{2\omega_s L} \quad (14)$$

where $\theta = \omega_s t$, with $\omega_s = 2\pi f_s$, and f_s the switching frequency. V'_{DC2} is the primary side referred DC output voltage.

B. Input Current and Power Flow

Currents $i_1(t)$ and $i_2(t)$ can be derived from $i_L(t)$ by analyzing the conduction states of the switches S_{xx} in respectively the primary and secondary side active bridges (Figs. 4(a) and 4(b)). Averaging $i_1(t)$ over one switching period $T_s = 1/f_s$ yields the expressions for the input current i_{DC1} and the input power P_1 :

$$i_{DC1} = \frac{1}{T_s} \int_0^{T_s} i_1(t) dt \quad (15)$$

Mode 1

$$i_{DC1} = \frac{dv_{DC1}}{2\omega_s L \pi} (2\phi\pi + 2\tau_1\pi - 2\tau_1\phi + 2\tau_2\phi + \tau_1\tau_2 - 2\phi^2 - \tau_1^2 - \tau_2^2 - \pi^2) \quad (16)$$

$$P_1 = \frac{dv_{DC1}^2}{2\omega_s L \pi} (2\phi\pi + 2\tau_1\pi - 2\tau_1\phi + 2\tau_2\phi + \tau_1\tau_2 - 2\phi^2 - \tau_1^2 - \tau_2^2 - \pi^2) \quad (17)$$

Mode 2

$$i_{DC1} = \frac{dv_{DC1}\tau_2(2\phi + \tau_1 - \tau_2)}{2\omega_s L \pi} \quad (18)$$

$$P_1 = \frac{dv_{DC1}^2\tau_2(2\phi + \tau_1 - \tau_2)}{2\omega_s L \pi} \quad (19)$$

where d is the primary side referred voltage conversion ratio:

$$d = \frac{V'_{DC2}}{v_{DC1}} \quad (20)$$

For realizing the unity power factor, i_{DC1} has to be controlled according to (1). The control equations for the phase shift angle ϕ can be found by combining equations (16) and (18) with (1):

Mode 1

$$\phi = \frac{-\tau_1}{2} + \frac{\tau_2}{2} + \frac{\pi}{2} \pm \sqrt{\frac{\tau_1\pi}{2} + \frac{\tau_2\pi}{2} - \frac{\tau_1^2}{4} - \frac{\tau_2^2}{4} - \frac{\pi^2}{4} - \frac{|I_{DC1} \sin(\omega_s t)|\omega_s L \pi}{V'_{DC2}}} \quad (21)$$

Mode 2

$$\phi = \frac{-\tau_1}{2} + \frac{\tau_2}{2} + \frac{|I_{DC1} \sin(\omega_s t)|\omega_s L \pi}{\tau_2 V'_{DC2}} \quad (22)$$

For mode 1 the "sqrt" solution should be taken, resulting in the lowest peak and RMS currents in the main components of the power circuit (i.e. the semiconductor devices, the HF AC-link, and the HF filter capacitors).

C. Soft-Switching Constraints

Zero-Voltage-Switching operation of the converter switches S_{xx} occurs when a voltage transition is initiated by turn-off of the respective transistor T_{xx} , transferring the total charge $Q_{oss,\Sigma}$ stored in the nonlinear parasitic output capacitance C_{xx} of the switch to the output capacitance of the opposite

switch of the leg. A minimum turn-off (commutation) current (primary side switches: $I_{p,comm}$, secondary side switches: $I_{s,comm}$) is needed to complete this resonant transition within the dead-time interval, avoiding shoot through and voltage transition delay, and imposing constraints on the inductor current i_L [12]. For both mode 1 and 2 the commutation instances are indicated by a "★" in Figs. 4(a) and 4(b) and the constraints for i_L are summarized in Table II. The constraint functions are determined by evaluating these constraints through expressions (7-14), yielding:

Mode 1

$$i_L(0, \pi) : \quad \phi \geq \frac{\tau_2}{2} - \frac{\tau_1}{2d} + \frac{I_{p,comm}\omega_s L}{V'_{DC2}} \quad (23)$$

$$i_L(\alpha) : \quad \phi \geq \pi - \tau_1 + \frac{\tau_2}{2} - \frac{\tau_1}{2d} + \frac{I_{p,comm}\omega_s L}{V'_{DC2}} \quad (24)$$

$$i_L(\beta) : \quad \phi \geq \pi - \frac{\tau_1}{2} - \frac{d\tau_2}{2} + \frac{\frac{n_2}{n_1} I_{s,comm}\omega_s L}{v_{DC1}} \quad (25)$$

$$i_L(\gamma) : \quad \phi \geq \tau_2 - \frac{\tau_1}{2} - \frac{d\tau_2}{2} + \frac{\frac{n_2}{n_1} I_{s,comm}\omega_s L}{v_{DC1}} \quad (26)$$

Mode 2

$$i_L(0, \pi) : \quad \tau_2 \leq \frac{\tau_1}{d} - \frac{2I_{p,comm}\omega_s L}{V'_{DC2}} \quad (27)$$

$$i_L(\alpha) : \quad \tau_2 \leq \frac{\tau_1}{d} - \frac{2I_{p,comm}\omega_s L}{V'_{DC2}} \quad (28)$$

$$i_L(\beta) : \quad \phi \geq \tau_2 - \frac{\tau_1}{2} - \frac{d\tau_2}{2} + \frac{\frac{n_2}{n_1} I_{s,comm}\omega_s L}{v_{DC1}} \quad (29)$$

$$i_L(\gamma) : \quad \phi \leq \frac{d\tau_2}{2} - \frac{\tau_1}{2} - \frac{\frac{n_2}{n_1} I_{s,comm}\omega_s L}{v_{DC1}} \quad (30)$$

For mode 1, as $0 \leq \tau_1 \leq \pi$, (23) is always satisfied when (24) is satisfied. Similarly (26) is always satisfied when (25) is satisfied. For mode 2 the soft-switching constraints at switching instances $\theta = 0$ (27) and $\theta = \alpha$ (28) are the same. These conclusions can easily be verified by analyzing the waveforms in Figs. 4(a) and 4(b). As a result, the soft-switching constraint functions for modes 1 and 2 can be condensed to (24) and (25) for mode 1, and (28), (29), and (30) for mode 2.

IV. CONTROL STRATEGY FOR FULL SOFT-SWITCHING, BIDIRECTIONAL, AC/DC OPERATION

In the previous section it was explained for mode 1 and mode 2 how the equations for the input current/power, as also the soft-switching constraint functions can be derived. This was done in a similar way for the six remaining modes for positive power flow. The implementation of the equations in the optimization/selection algorithm mentioned in Section III and the analysis of the outcome led to the strategy that allows to control the DAB AC/DC converter under full ZVS (i.e. in the whole voltage and power range). In the following, the control strategy, which is finally based on switching modes 1 and 2 only, is explained using Fig. 5 by moving step by step through the 50Hz sinewave interval and considering

TABLE II
SOFT-SWITCHING CONSTRAINTS

| i_L | Mode 1 | Mode 2 |
|----------------------|---|---|
| $i_L(0) = -i_L(\pi)$ | $\leq -I_{p,comm}$ Prim. bridge | $\leq -I_{p,comm}$ Prim. bridge |
| $i_L(\alpha)$ | $\leq -I_{p,comm}$ | $\leq -I_{p,comm}$ |
| $i_L(\beta)$ | $\geq \frac{n_2}{n_1} I_{s,comm}$ Sec. bridge | $\geq \frac{n_2}{n_1} I_{s,comm}$ Sec. bridge |
| $i_L(\gamma)$ | $\geq \frac{n_2}{n_1} I_{s,comm}$ | $\leq \frac{n_2}{n_1} I_{s,comm}$ |

the currents in the primary and secondary side switches at the different switching instances $\theta = \{\alpha, \beta, \gamma, \text{ and } \pi\}$ ($i_{s,p}$ and $i_{s,s}$ in respectively Fig. 5(a) and Fig. 5(b)). It should be reminded that the primary side switches commute at instances $\theta = \{\alpha, \pi\}$, while the secondary side switches commute at instances $\theta = \{\beta, \gamma\}$. In order to achieve full ZVS, the constraints depicted in Table II have to be met during the whole sinewave interval. In a next step, Fig. 5(c) is used to explain how the transformer magnetizing inductance L_M can facilitate commutation current in the secondary side switches around mode transition. The explanatory curves are derived for the minimum AC input voltage $V_{AC,rms} = 207V$, the minimum DC output voltage $V_{DC2} = 360V$, and the nominal AC input current $I_{AC,rms,nom} = 16A$ (i.e. the most critical operating condition). A minimum commutation current of $I_{p,comm} = I_{s,comm} = 2A$ is assumed for both the primary and secondary side high-frequency switches. For clarity, in each figure only a quarter of the 50Hz period is shown.

A. Quasi Full Soft-Switching Operation

It was seen from the optimization/selection algorithm that in the beginning of the 50Hz sinewave interval mode 2 is preferably used (interval A-D, Fig. 5), turning into mode 1 in a second interval (D-F). For convenience, the explanation starts in point B of the 50Hz interval. The resulting control angles for the considered operating condition are shown in Fig. 6 (solid lines).

• Interval B-C: mode 2a

During interval B-C, the commutation current in the primary side switches is exactly equal to the one that is minimum required, $i_{s,p}(\alpha) = -I_{p,comm} = -2A$ and $i_{s,p}(\pi) = I_{p,comm} = 2A$. The same can be remarked for the commutation current $i_{s,s}(\gamma) = -I_{s,comm} = -2A$ in the secondary side switches. This condition can be achieved by replacing the " \leq " by a " $=$ " in equations (28) and (30), and by combining them to eliminate τ_1 and τ_2 , yielding the expression for ϕ (Table III, mode 2a). The expression for ϕ can be used in (22), and combined with (28) to find the expressions for τ_1 and τ_2 (Table III, mode 2a). Since $i_{s,s}(\beta) > 2A$, all soft-switching constraints according to Table II are satisfied. It can be analytically verified that the resulting quasi triangular shaped inductor current gives the minimum RMS switch current.

• Interval C-D: mode 2b

From point C of the 50Hz period, the result of the equation for τ_1 (Table III, mode 2a) is $> \pi$, being physically impossible.

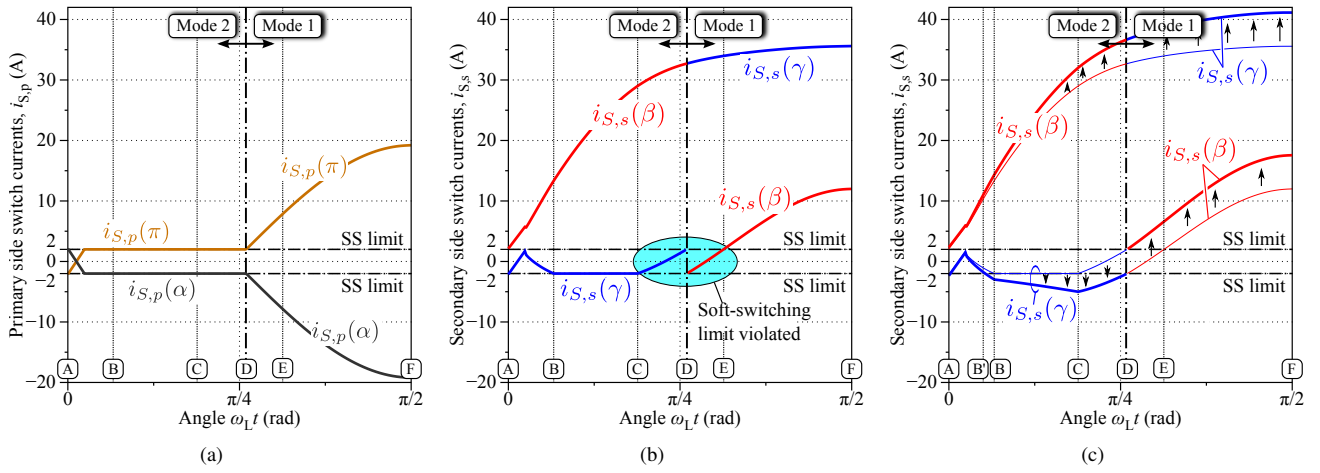


Fig. 5. Primary side switch commutation currents (Fig. 5(a)), secondary side switch commutation currents without consideration of the transformer magnetizing inductance L_M (Fig. 5(b)), and secondary side switch commutation currents with consideration of the transformer magnetizing inductance L_M (Fig. 5(c)).

From this point the soft-switching constraints for mode 2 can not all be met, causing the algorithm to select the inefficient mode 5 (not shown in Fig. 5). However the abrupt mode transition would introduce an unwanted dynamic behaviour and therefore it was chosen to continue in the more efficient mode 2, clipping τ_1 to π (smooth transition). As a result, τ_2 is calculated with (28), replacing the " \leq " by a "=", and ϕ with (22) (Table III, mode 2b). Now the commutation current in the primary side switches still equals the minimum required commutation current, $i_{S,p}(\alpha) = -I_{p,comm} = -2A$ and $i_{S,p}(\pi) = I_{p,comm} = 2A$, while $i_{S,s}(\gamma)$ increases towards zero (i.e. soft-switching constraint (30) for the secondary side switches is violated).

• Interval D-F: mode 1

At point D, ϕ becomes zero (transition from mode 1 to mode 2). However, as the soft-switching constraints for mode 1 can not all be met during interval D-E, from the algorithm it was observed that inefficient mode 5 (not shown in the figure) is selected instead of mode 1. For the same reason as explained above it was chosen to continue with mode 1 and meeting only the primary side commutation constraints. It can be seen from equation (24) that this can be achieved by calculating τ_2 according to Table III, mode 1, knowing that τ_1 is still clipped to π (smooth transition) and that for mode 1, $\phi \geq 0$. ϕ is then calculated with (21). The commutation currents $i_{S,p}(\pi)$ and $i_{S,p}(\alpha)$ in the primary side switches meet the soft-switching constraints during the whole interval D-F and are equal to the minimum required commutation current in point D. Note that the abrupt line transition at $\phi = 0$ in Fig. 5 is because of the definition of angles β and γ in Figs. 4(a) and 4(b), while the real converter currents experience a smooth transition. The soft-switching constraint (25) for the secondary side switches is violated. However, at a certain point E, $i_{S,s}(\beta) > 2A$ and again full soft-switching is achieved. The control angles for mode 1 (according to Table III, mode 1) slightly differ from the ones obtained with the optimization/selection algorithm, resulting in a suboptimal (close to optimal) switch RMS

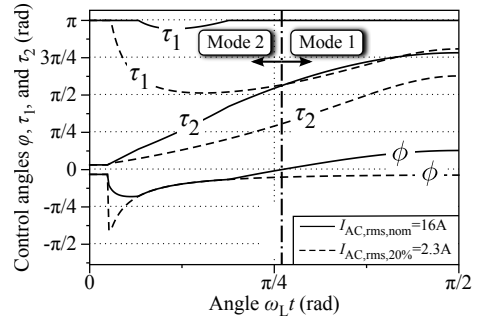


Fig. 6. DAB control angles ϕ , τ_1 , and τ_2 for nominal (solid), and 20% of nominal (dashed) power.

current. The expressions for the angles that give the real optimum could not be presented due to length restrictions but will be given in the transactions version of the paper.

It can be concluded that when calculating the control angles ϕ , τ_1 , and τ_2 according to Table III, the soft-switching constraints in the primary side switches are met during the whole 50Hz period. However, during a small interval (C-E) around the mode transition, soft-switching in the secondary side switches is not achieved (Fig. 5(b)). Theoretically in interval C-E full soft-switching is only possible when assuming zero switch commutation current, $I_{p,comm} = I_{s,comm} = 0A$, resulting in increased switching losses. This problem can be solved by considering the magnetizing inductance L_M of the HF transformer, using the Pi-equivalent circuit (Fig. 7) of the HF AC-link as explained in the next section. It should be noted that during a very small interval (A-B) of the 50Hz period soft-switching can not be achieved. However, this does not cause increased losses as in this interval the current i_{DC1} is almost zero anyway. During interval A-B, the control angles are also calculated according to Table III, mode 2b, taking into consideration the same remarks as for interval C-D. For low power levels (Fig. 6, dashed lines) mode 1 will not be entered and only mode 2a used.

TABLE III
EXPRESSIONS FOR THE MODULATION ANGLES τ_1 , τ_2 , AND ϕ FOR ACHIEVING FULL SOFT-SWITCHING, BIDIRECTIONAL AC/DC OPERATION.

| | Mode 2 | | Mode 1 |
|----------|--|--|--|
| | 2a | 2b | |
| τ_1 | $\frac{2d\omega L}{v_{DC1}-V_{DC2}'} \left(I_{p,comm} \left(\frac{1}{d} - 1 \right) - \frac{n_2 I_{s,comm}}{2} - \sqrt{\frac{\left(\frac{n_2}{n_1} I_{s,comm} \right)^2}{4} + \frac{\pi i_{DC1} v_{DC1} (1 - \frac{1}{d})}{2\omega L}} \right)$ | π | π |
| τ_2 | $\frac{2\omega L}{v_{DC1}-V_{DC2}'} \left(-\frac{n_2 I_{s,comm}}{2} - \sqrt{\frac{\left(\frac{n_2}{n_1} I_{s,comm} \right)^2}{4} + \frac{\pi i_{DC1} v_{DC1} (1 - \frac{1}{d})}{2\omega L}} \right)$ | $\frac{\tau_1}{d} - \frac{2\omega L I_{p,comm}}{V_{DC2}'}$ | $\frac{\tau_1}{d} - \frac{2\omega L I_{p,comm}}{V_{DC2}'}$ |
| ϕ | $\frac{\omega L (I_{p,comm} + \frac{n_2}{n_1} I_{s,comm})}{v_{DC1}}$ | Eqn. (22) | Eqn. (21) |

B. Full Soft-Switching Operation by Inclusion Of the Transformer Magnetizing Inductance L_M

The magnetizing inductance L_M of the HF transformer can be used to achieve soft-switching in the secondary side switches during the small interval (C-E) around the mode transition. Therefore the Pi-equivalent circuit (depicted in Fig. 7) of the HF AC-link is used, where the inductance values can be calculated with:

$$L_{XY} = L + L_{tr1} + (n_1/n_2)^2 L_{tr2} + \frac{(L + L_{tr1}) \cdot (n_1/n_2)^2 L_{tr2}}{L_M} \quad (31)$$

$$L_{XZ} = L + L_{tr1} + L_M + \frac{(L + L_{tr1}) \cdot L_M}{(n_1/n_2)^2 L_{tr2}} \quad (32)$$

$$L_{YZ} = L_M + (n_1/n_2)^2 L_{tr2} + \frac{(n_1/n_2)^2 L_{tr2} \cdot L_M}{L + L_{tr1}} \quad (33)$$

When the transformer leakage inductances are neglected ($L_{tr1} = L_{tr2} = 0$), the equations simplify to $L_{XY} = L$, $L_{XZ} = \infty$, and $L_{YZ} = L_M$. The current in the secondary side switches $i_{s,s}(t)$ can now be determined by applying Kirchoff's current law to node Y,

$$i_{s,s}(t) = \frac{n_1}{n_2} i'_{s,s}(t) = \frac{n_1}{n_2} (i_L(t) - i_{YZ}(t)) \quad (34)$$

By analyzing the primary side referred voltage v'_2 in Figs. 4(a) and 4(b) it can be seen that the current i_{YZ} in the transformer magnetizing inductance L_M always has a beneficial contribution to the commutation currents $i_{s,s}(\beta)$ and $i_{s,s}(\gamma)$ in the secondary side switches (Fig. 5(c)), while having no influence on the current $i_{s,p}$ in the primary side switches. It can be shown that when calculating L_M with (35) (Appendix), also the minimum commutation current in the secondary side switches is satisfied during the small interval (C-E) around the mode transition (Fig 5(c)), achieving ZVS operation over the whole input sinewave interval and power range of the DAB AC/DC converter. The derivation of the equation for L_M (critical operating condition) could not be presented in the paper due to length restrictions but, however, will be given in the transactions version of the paper.

V. EXPERIMENTAL RESULTS AND TOPOLOGY EVALUATION

A prototype of the full bridge - full bridge DAB AC/DC converter was in its final design phase at the moment of

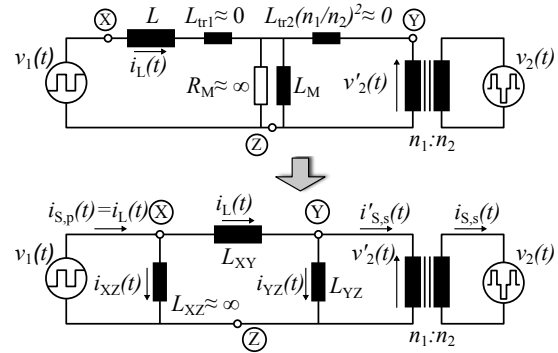


Fig. 7. Pi-equivalent circuit of the HF AC-link (inductor-transformer).

writing this paper. However, the proposed strategy to control this converter under full soft-switching is an extension on previous work [11], where the analysis was performed for a half bridge - full bridge DAB implementation. Despite the fact that with the full bridge - full bridge DAB more flexibility is provided to shape the inductor current i_L and minimize the component RMS currents, the basic control principle stays the same. Therefore, to validate the proposed strategy, the results obtained with the half bridge - full bridge prototype of [11] are briefly summarized in Fig. 8. The inset shows

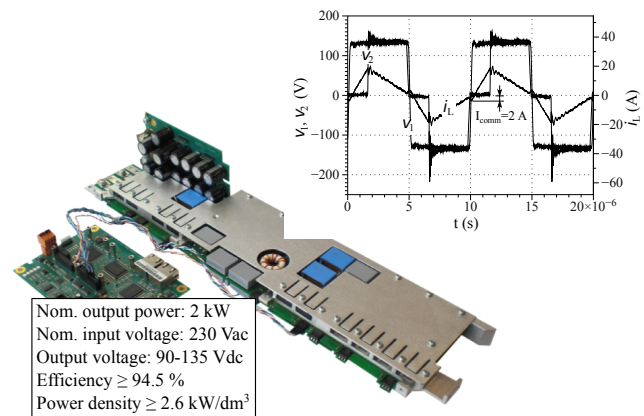


Fig. 8. Single-stage, bidirectional, half bridge-full bridge DAB AC/DC converter prototype.

that a commutation current of 2A is achieved in the critical operating point (i.e. at the mode transition). A high converter efficiency of >94% was achieved at both the nominal and minimum output voltage.

In order to investigate the potential (in terms of efficiency and power density) of the single-stage DAB AC/DC converter concepts (the Single Stage Full bridge - Full bridge DAB (SSFF converter) analyzed in this paper on the one hand and the Single Stage Half bridge - Full bridge DAB (SSHF converter) analyzed in [11] on the other hand), a comprehensive comparative evaluation was performed in [14], considering also a state-of-the-art conventional Dual-Stage (DS converter) concept (i.e. a bidirectional interleaved triangular current mode (TCM) PFC rectifier in combination with a DAB DC/DC converter). The comparison is based on common system specification (Table I) and showed the highest nominal efficiency for the DS, while in partial load the SSFF outperforms the DS converter (Fig. 9). The SSHF has the lowest overall efficiency. Concerning component count and power density, the single-stage concepts are advantageous as they use less active components and show a lower volume for the passive components, being also a cost and reliability advantage.

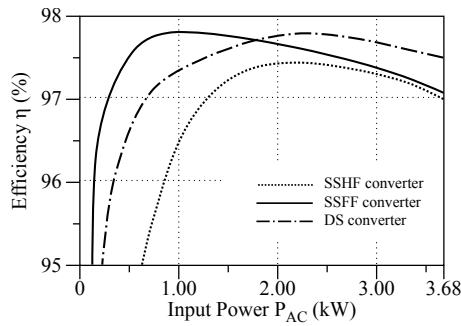


Fig. 9. Calculated efficiency of the SSHF, the SSFF, and the DS converters [14].

VI. CONCLUSION

A switching control strategy to enable soft-switching operation of a full bridge - full bridge DAB AC/DC converter in the entire input sinewave interval and full power range is presented. An analysis of the possible switching modes is provided from which a selection of two "most feasible" modes is made. The final switching control strategy combines these two modes in an appropriate way in order to achieve full soft-switching AC/DC operation and unity power factor. It is shown that both active bridges can operate with a finite commutation current, enhancing the resonant transition at transistor turn-off. Hereby the magnetizing inductance of the transformer is used to facilitate commutation current in the secondary bridge. Although the theoretical analysis of the proposed strategy requires much effort, the final control equations and design rules are relatively simple. This, together with the promising results obtained from a comprehensive system comparison, makes the single - stage full bridge-full bridge DAB a feasible solution for isolated, bidirectional AC/DC applications.

REFERENCES

- [1] A. Stupar, T. Friedli, J. Miniböck, M. Schweizer, and J. W. Kolar, "Towards a 99% Efficient Three-Phase Buck-Type PFC Rectifier for 400 V DC Distribution Systems," in *IEEE 26th Applied Power Electronics Conference and Exposition (APEC 2011)*, March 2011, pp. 505–512.
- [2] A. Pratt, P. Kumar, and T. V. Aldridge, "Evaluation of 400 V DC Distribution in Telco and Data Centers to Improve Energy Efficiency," in *29th International Telecommunications Energy Conference (INTELEC 2007)*, Oct. 2007, pp. 32–39.
- [3] A. Matsumoto, A. Fukui, T. Takeda, and M. Yamasaki, "Development of 400-Vdc Output Rectifier for 400-Vdc Power Distribution System in Telecom Sites and Data Centers," in *32nd International Telecommunications Energy Conference (INTELEC 2010)*, June 2010, pp. 1–6.
- [4] A. Emadi, S. S. Williamson, and A. Khaligh, "Power Electronics Intensive Solutions for Advanced Electric, Hybrid Electric, and Fuel Cell Vehicular Power Systems," *IEEE Transactions on Power Electronics*, vol. 21, no. 3, pp. 567–577, May 2006.
- [5] K. Clement-Nyns, E. Haesen, and J. Driesen, "The Impact of Vehicle-to-Grid on the Distribution Grid," *Electric Power Systems Research*, vol. 81, no. 1, pp. 185–192, 2011. [Online]. Available: <http://www.sciencedirect.com/science/article/pii/S0378779610002063>
- [6] Directorate-General for Research and Innovation, European Commission. (2005) Towards Smart Power Networks, Lessons Learned from European Research FP5 Projects. [Online]. Available: http://ec.europa.eu/research/energy/eu/publications/index_en.cfm
- [7] R. W. De Doncker, D. M. Divan, and M. H. Kheraluwala, "A Three-Phase Soft-Switched High Power Density DC/DC Converter for High Power Applications," in *IEEE Industry Applications Society Annual Meeting*, vol. 1, Oct. 1988, pp. 796–805.
- [8] M. H. Kheraluwala and R. W. De Doncker, "Single Phase Unity Power Factor Control for Dual Active Bridge Converter," in *IEEE Industry Applications Society Annual Meeting*, vol. 2, Oct. 1993, pp. 909–916.
- [9] G. G. Oggier, R. Ledhold, G. O. Garcia, A. R. Oliva, J. C. Balda, and F. Barlow, "Extending the ZVS Operating Range of Dual Active Bridge High-Power DC-DC Converters," in *IEEE 37th Power Electronics Specialists Conference (PESC 2006)*, June 2006, pp. 1–7.
- [10] G. G. Oggier, G. O. Garcia, and A. R. Oliva, "Switching Control Strategy to Minimize Dual Active Bridge Converter Losses," *IEEE Transactions on Power Electronics*, vol. 24, no. 7, pp. 1826–1838, July 2009.
- [11] J. Everts, J. Van den Keybus, and J. Driesen, "Switching Control Strategy to Extend the ZVS Operating Range of a Dual Active Bridge AC/DC Converter," in *IEEE Energy Conversion Congress and Exposition (ECCE 2011)*, Sept. 2011, pp. 4107–4114.
- [12] F. Krismer and J. W. Kolar, "Accurate Power Loss Model Derivation of a High-Current Dual Active Bridge Converter for an Automotive Application," *IEEE Transactions on Industrial Electronics*, vol. 57, no. 3, pp. 881–891, March 2010.
- [13] S. Waffler and J. W. Kolar, "Comparative Evaluation of Soft-Switching Concepts for Bi-Directional Buck+Boost DC-DC Converters," in *International Power Electronics Conference (IPEC 2010)*, June 2010, pp. 1856–1865.
- [14] J. Everts, F. Krismer, J. Van den Keybus, J. Driesen, and J. W. Kolar, "Comparative Evaluation of Soft-Switching, Bidirectional, Isolated AC/DC Converter Topologies," in *IEEE 27th Applied Power Electronics Conference and Exposition (APEC 2012)*, Feb. 2012.

APPENDIX

$$L_M = \frac{1}{2\omega(I_{p,comm} + \frac{n_2}{n_1} I_{s,comm})} \left(\frac{1}{2V_{DC1,min}^2 \pi^2} (V_{DC1,min} \pi \cdot (4\omega L \pi V_{DC1,min} I_{p,comm} - 2\omega L \pi I_{DC1,max} V'_{DC2,min} + \pi^2 V_{DC1,min} \cdot V'_{DC2,min} + (4\omega^2 L^2 \pi^2 I_{DC1,max}^2 V_{DC2,min}^2 - 16\omega^2 L^2 \pi^2 I_{DC1,max}^2 \cdot V'_{DC2,min} V_{DC1,min} I_{p,comm} - 4\omega L \pi^3 I_{DC1,max} V_{DC2,min}^2 V_{DC1,min} + \pi^4 V_{DC2,min}^2 V_{DC1,min}^2)^{1/2}) - 2I_{p,comm}) \right) \quad (35)$$